Cement & Concrete Composites 32 (2010) 92–99

Contents lists available at ScienceDirect

Cement & Concrete Composites

journal homepage: www.elsevier.com/locate/cemconcomp

Discussion

Does microstructure matter for statistical nanoindentation techniques? ☆

Franz-Josef Ulm [a,*], Matthieu Vandamme [b], Hamlin M. Jennings [c], James Vanzo [a], Michelle Bentivegna [a], Konrad J. Krakowiak [d], Georgios Constantinides [e], Christopher P. Bobko [f], Krystyn J. Van Vliet [a]

[a] Massachusetts Institute of Technology, Cambridge, MA, United States
[b] Université Paris-Est, Ecole des Ponts ParisTech–UR Navier, France
[c] Northwestern University, Evanston, IL, United States
[d] University of Minho, Guimarães, Portugal
[e] Cyprus University of Technology, Cyprus
[f] North Carolina State University, Raleigh, NC, United States

ARTICLE INFO

Article history:
Received 27 August 2009
Received in revised form 29 August 2009
Accepted 31 August 2009
Available online 6 September 2009

Keywords:
Nanoindentation
Statistical analysis
Microstructure

ABSTRACT

In their paper, Trtik et al. (2009) identify spurious peaks in the application of statistical nanoindentation technique as a critical obstacle for mechanical phase identification. In this discussion, we show that Trtik et al.'s finding is a consequence of an unrealistic virtual 3-D checkerboard microstructure considered by the authors. These peaks are not a general feature of indentation on multiphase materials, nor can the presence of such peaks be attributed to an intrinsic shortcoming of the grid-indentation technique. We also show that the authors' assertion of the absence of homogeneous material regions extending beyond 3 μm in cementitious materials is groundless.

1. Introduction

One of the most promising techniques that emerged from the implementation of nanotechnology in materials science and engineering to assess mechanical properties at small scales is nanoindentation. The idea is simple: by pushing a needle onto the surface of a material, the surface deforms in a way that reflects the mechanical properties of the indented material. Yet, in contrast to most metals and ceramics, for which this technique was originally developed, most materials relevant for civil engineering, petroleum engineering or geophysical applications, are highly heterogeneous and multi-phase materials from a scale of a few nanometers to macroscopic scales. This brought about statistical nanoindentation techniques [1–4]: by carrying out a large array of nanoindentation tests on a surface of a multi-phase material, mechanically active phases are identified by statistical means. The technique consists of fitting a mixture model of multivariate normal distributed components to the experimental nanoindentation data set (indentation modulus M, indentation hardness H). A typical example is shown in Fig. 1.

In an article, Trtik et al. (2009) add a new dimension to the discussion: virtual nanoindentation experiments on a three-dimensional checkerboard, sought to represent a two-phase microstructure. By averaging the elastic moduli of voxels (volumetric pixels) within a cubic interaction volume randomly placed at various locations over the virtual checkerboard, an estimate of the elastic modulus is obtained that is considered to represent the elastic modulus measured by an indentation at this location. The statistical analysis of the elastic moduli so obtained then reveals that the elasticity content of the two-phase virtual material can only be correctly depicted if the characteristic size of the phases, say D, is 10 times the size of indentation depth h that activates an interaction volume of $d = 3–4h$.

It is not difficult to confirm these calculations analytically: consider Trtik et al.'s 3-D ("black–white") checkerboard microstructure of checker edge size D, such that the total edge size of the board is jD, with $j = 2m$ ($m = 1,2,3,\ldots$). Let $j^3/2$ be the number of boxes per phase (black or white) in the volume, such that the volume fraction of each phase is 50%. Let the 3-D checkerboard be probed by a marching object of size d. The probability of probing one of the pure phases is proportional to the volume fraction $V_1/V_{\lim} = V_2/V_{\lim} = 1/2$, where $V_{\lim} = (jD)^3$. The actual volume, however, of possible locations of virtual nanoindentations of non-zero size d is $V = (jD - d)^3$, satisfying $\lim_{d\to 0} V = V_{\lim}$. As a

☆ A Discussion of the paper 'A critical examination of nanoindentation on model materials and hardened cement pastes based on virtual experiments', by Trtik, Münch and Lura, Cement and Concrete Composites, doi:10.1016/j.cemconcomp.2009.07.001.

* Corresponding author.
E-mail address: ulm@mit.edu (F.-J. Ulm).

0958-9465/$ - see front matter © 2009 Elsevier Ltd. All rights reserved.
doi:10.1016/j.cemconcomp.2009.08.007

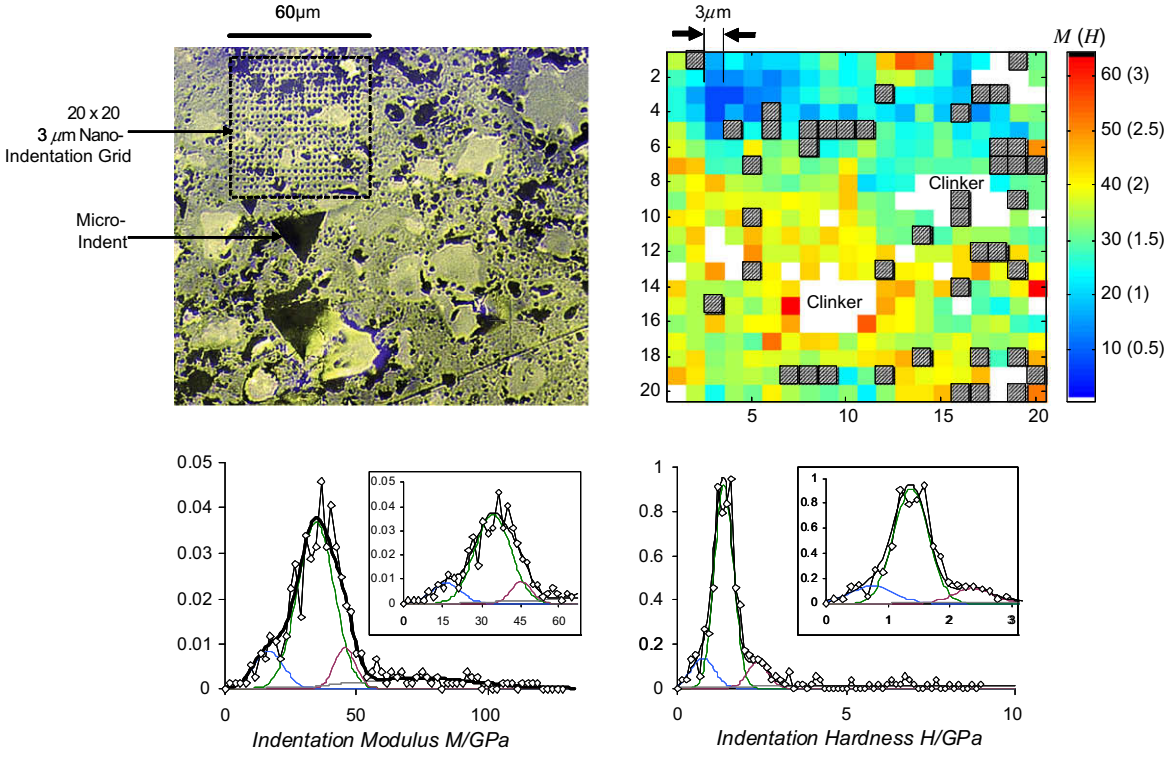

Fig. 1. Grid-Indentation test on $w/c = 0.3$ cement paste with a 3 μm spaced 20×20 grid (clockwise): optical microscope image of indentation grid; mapping of nanomechanical properties showing homogenous material regions of same properties (the hatched boxes are removed tests recognized through irregularities in indentation response (here 43/400) arising mostly at locations of indentation on capillary porosity or defects at hard–soft interfaces). Probability density and deconvolution of indentation modulus M and indentation hardness H in four phases (LD C–S–H, HD C–S–H, UHD, and clinker). Hydration products have an indentation modulus smaller than 65 GPa, and a strength (hardness) smaller than 3 GPa, as shown by atomistic simulations [31].

consequence, the actual volume of each phase ("black" or "white") sampled by such a finite sized marching object is $V_1 = \frac{1}{2}j^3(D-d)^3$, while the remaining volume, $V_{12} = V - 2V_1$, is the one sampled by the marching object along interface zones where the material is a mixture ("gray"). The probability of sampling one of the pure phases thus is $P_1 = P_2 = V_1/V$, while the probability of sampling a composite point is $P_{12} = V_{12}/V = 1 - 2P_1$. A bi-modal distribution will thus be favored, if $2P_1 > P_{12}$. This implies for Trtik et al.'s choice of $j = 4$ and of $D = 32$ (shown both in Fig. 2 of their paper), that $d < 8$ would ensure a bi-modal distribution. Hence, these simple back-of-the envelope calculations readily confirm the authors' finding that (cit.) "the bi-modality of the distribution disappears completely for the size of the cube of $[d^3 =]12^3$ voxels". More generally, imposing a restriction on the probabilities $2P_1/P_{12} > 1$ comes to restrict the D/d ratio as a function of the checkerboard size j. For instance, for $j = 4$, bi-modality requires $D/d > 3.9$, or equivalently $D/h > 12$ (if we let $d = 3h$). One could argue that Trtik et al.'s simulations (and thus conclusions) are size dependent, as the limit value of D/d depends on j, the number of checkers along any edge of the 3-D checkerboard. This dependence on size can be removed by an asymptotic analysis, $j \to \infty$. In this case, the criterion for bi-modality, $\lim_{j\to\infty}(2P_1/P_{12}) > 1$, entails $D/d > 4.8$ or $D/h > 15$.

This criterion for mechanical phase separability is reminiscent of Buckle's rule-of-thumb [5]: for a heterogeneous material, Buckle's rule-of-thumb ensures that tools of continuum indentation analysis based on the Hertz contact solution [6–10], which link indentation measurements (typically a force–indentation depth curve) to meaningful elasticity properties of the indented half-space, can be employed with some confidence. Employing the thin-film analogy, Constantinides et al. confirmed this phase separability condition, showing that $D/h > 10$ ensures that the elastic properties of the indented composite does not diverge more than 10% from the elastic properties of the (thin film) phase [1]. Trtik et al. thus contribute to the discourse by showing that the same holds true for a checkerboard microstructure; as it does, as we will show below, for an inclusion–matrix morphology. That is, Buckle's rule-of-thumb holds irrespective of the particular microstructure.

While this conclusion is far from original, truly new is the finding that for smaller D/h ratios, no clear (mechanical) phase separation is statistically possible due to the presence of spurious peaks that render the possibility of identifying material phases by means of statistical analysis of elasticity properties erroneous. Based on these virtual observations, the authors question our previous identification of the mechanical properties of two compositionally similar but structurally distinct C–S–H phases, namely low density (LD) C–S–H and high density (HD) C–S–H [11,2,12]; and more generally caution the use of statistical indentation technique for cement paste materials whose microstructure – according to the authors – does not display large enough sized areas to meet the identified criteria for phase separation. The authors also question some surface roughness issues for surface preparation proposed by us earlier [13]; but these questions derive rather from their method of surface preparation for focussed ion beam nanotomography than from our procedure validated by means of statistical nanoindentation.

The questions raised in this paper are challenging. Whether or not the authors' conclusions are of general nature, or rather tainted by the particular choice of model and virtual microstructure is the focus of this discussion. Otherwise said: Does microstructure matter for statistical indentation analysis?

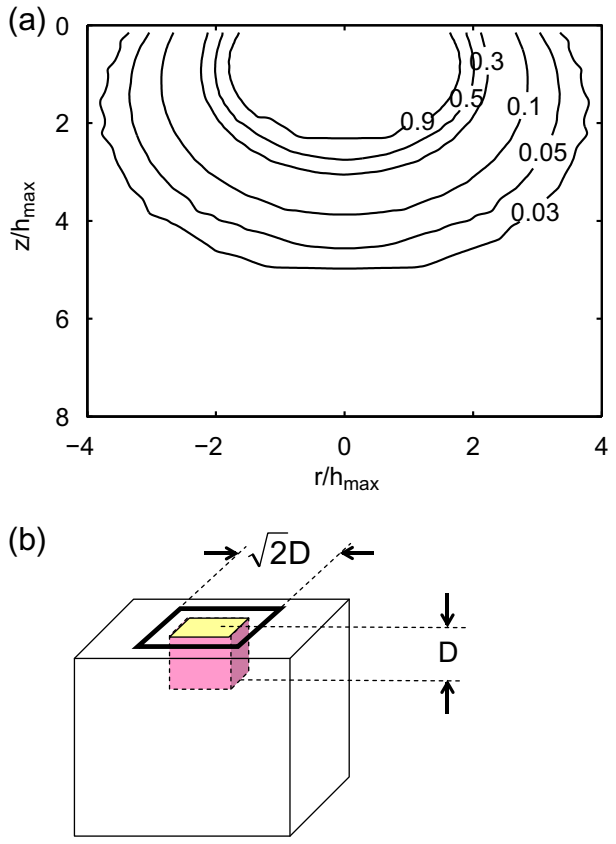

Fig. 2. Virtual indentation analysis on a model material: (a) iso-contours of the normalized local strain energy density obtained from finite element calculation of the indentation of an elastoplastic half-space under axisymmetrical conditions. The Berkovich tip was approximated by a cone of half-angle 70.3°. The strength properties of the indented material (yield strength–to–modulus ratio of $10^{-1.5}$) were chosen such that the computed contact depth-to-indentation depth ratio (h_c/h_{max}) is close to the experimentally measured value in cement paste nanoindentation, $h_c/h_{max} = 0.88$. For different D/h_{max} ratios, this normalized strain density field is superimposed on (*b*) the inclusion–matrix microstructure in the calculation of the "effective" modulus for randomly chosen locations of the indenter situated on a surface twice the size of the inclusion surface.

2. Hypothesis testing

Let us assume –with Trtik et al.– that the authors' conclusions hold for any microstructure. Spurious peaks in statistical nanoindentation should then occur for any multiphase material morphology, including a matrix-inclusion morphology which more realistically depicts the microstructure of hydrated multiphase materials, such as cement pastes (e.g. clinker rimmed by High-Density C–S–H within a Low-Density C–S–H matrix). In order to test the hypothesis, we repeated the same type of virtual nanoindentation experiments proposed by the authors, but with two modifications:

- Instead of considering a 3-D checkerboard, we considered a unique inclusion embedded into a matrix (Fig. 2b). Virtual indentations were performed on the surface at random locations. In order to probe reasonably often the inclusion, virtual nanoindentations were restricted to the surface of the inclusion and its vicinity, such that the whole surface made available for virtual indentations was twice the apparent surface of the inclusion. Distinct values of elastic modulus (of sufficient contrast) were given to the matrix and to the inclusion.
- Instead of considering a cubic interaction volume, we consider a more realistic interaction volume defined by strain energy gradients below the indenter. Indeed, from a straightforward application of micromechanics principles [14], it is readily recognized that Trtik et al.'s procedure of averaging the moduli in a cubic volume comes to assume that the entire material within the cubic interaction volume exhibits the same strain field (similar to the Voigt upper bound or mixture model), such that the material close to the indenter contributes to the "effective" modulus the same way as a material at the lower end of the cubic interaction volume. Real indentation interaction volumes are of a different nature, as well known from the elastic stress and strain field solutions [7–10] and as finite element simulations show (Fig. 2a): the strain energy, which is a measure of the level of elastic material activation, decreases in half-spheres with the radial distance. Thus, in order to account for a more realistic gradation in the level of material activation with strain level within a realistic interaction volume, we superimpose, at the location of each virtual nanoindentation, the strain energy density field (Fig. 2a) on the virtual microstructure (Fig. 2b) and use it as a weighing function in the elastic modulus averaging process (analogously to strain localization in linear micromechanics). For each indentation depth considered (fixed D/h_{max} ratio), 1000 such virtual indentations were performed.

The simulated frequency plots are displayed in Fig. 3. The results confirm both the validity of Buckle's rule–of–thumb for any microstructure, and the very foundation of the grid-indentation technique: shallow indents (large D/h_{max}) allow a clear phase separation (represented by the two peaks in the two-phase composite), while deep indents (small D/h_{max}) lead to a homogenized response represented by one peak. Furthermore, in contrast to Trtik et al.'s conjecture, at no indentation depth do we observe spurious peaks. Otherwise said, such spurious peaks appear to us a consequence of Trtik et al.'s particular microstructure, the 3-D checkerboard. In fact, we also simulated the 3-D checkerboard microstructure using the same principle of superposition for averaging the elastic modulus, and found indeed the occurrence of a spurious peak for $D/h_{max} < 10$ (Fig. 4). But clearly, such spurious peaks are not a general feature of indentation on multiphase materials, nor can their occurrence be attributed to an intrinsic failure of the grid-indentation technique, but rather to the choice by Trtik of an ad hoc microstructure.

It is thus not surprising that we have not observed such spurious peaks in statistical nanoindentation, not in cement paste nanoindentation [2,3,15,13,16], nor in bone nanoindentation [17,3], shale nanoindentation [18,19] or nanoindentation on titanium–titanium monoboride (Ti–TiB) composites [1], nor in other two phase and three phase engineered composite materials (2-phase $\alpha - \beta$ brass, 3-phase cast iron (graphite, martensite, and carbide), 2-phase Ti64-10TiC composite, and so on) [4].

This robustness of the statistical nanoindentation technique is additionally enhanced by the simultaneous consideration of two measured indentation quantities, M and H (see Fig. 1), the first relating to the elasticity, the second to the strength properties of the indented phases [20–22]. In fact, while Buckle's rule-of-thumb, $D/h > 10$, satisfies elastic homogeneity (which is the focus of Trtik et al.'s discussion), for hardness, from simulations of conical indentations on (almost) rigid perfectly plastic biphasic systems considering different inclusion morphologies (particle embedded in a matrix, thin film on a substrate), Durst et al. [23] showed that $D/h > \max(4; 2\cot\theta)$ (where $\theta = 70.32°$ is the equivalent cone angle representative of the Berkovich indenter) was sufficient to measure correctly the indentation hardness (and thus strength properties) of the inclusion phase. This means that the material volume solicited elastically below the indenter is much larger than the volume solicited plastically. Given this difference in material volume solicited respectively elastically and plastically,

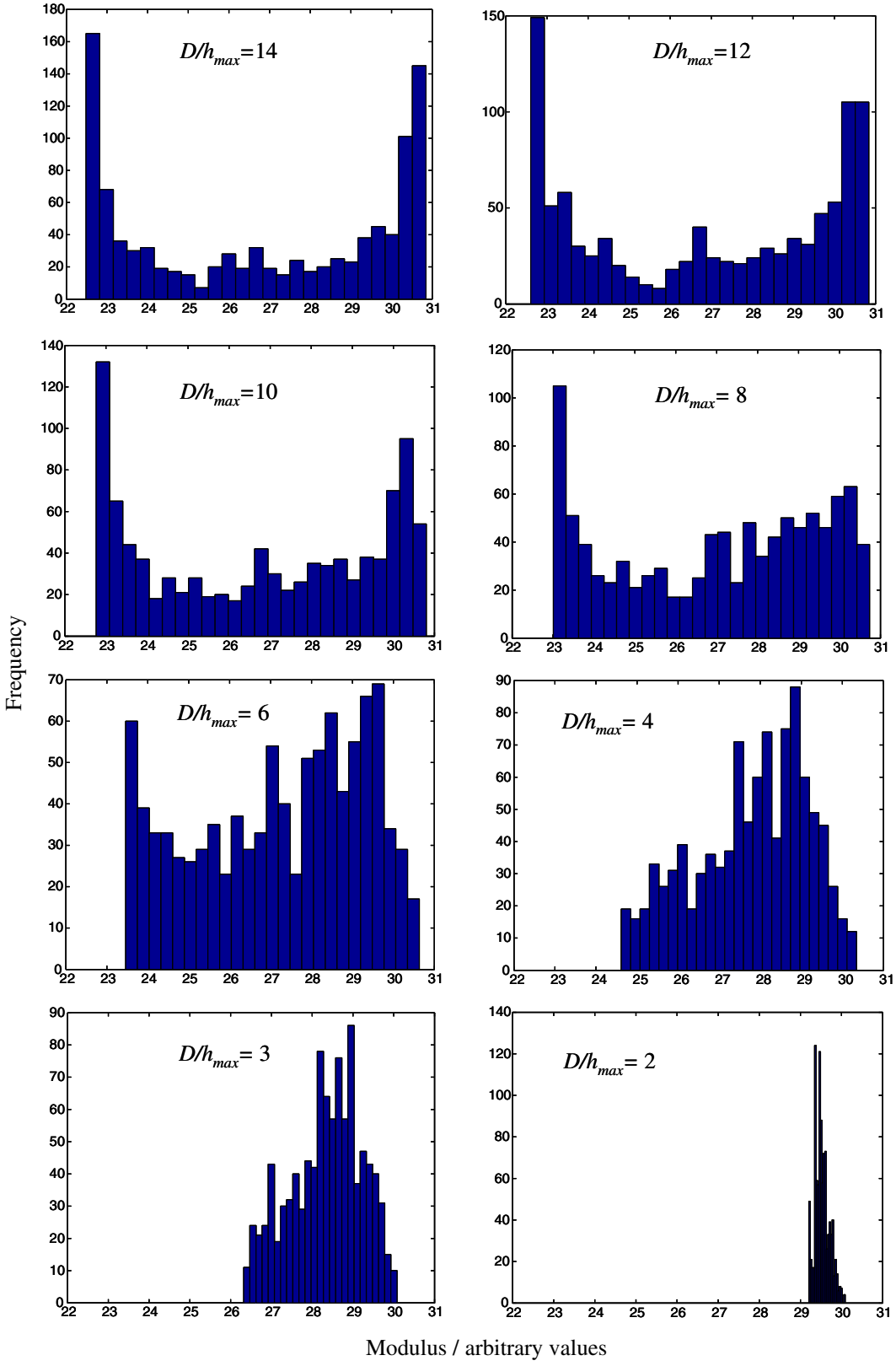

Fig. 3. Frequency plots of random indentation on a two-phase matrix-inclusion material for different inclusion size -to- indentation-depth ratios, D/h_{max}. The figures confirm the well known homogenization effect without spurious peaks with an increase of the indentation depth.

the simultaneous consideration of M and H in the analysis is expected to add some robustness to the technique that strongly aids the identification of mechanically activated material phases by grid-indentation. In our simulations, we implicitly considered the elastoplastic nature of the half-space, by determining the interaction volume from elastoplastic finite element simulations

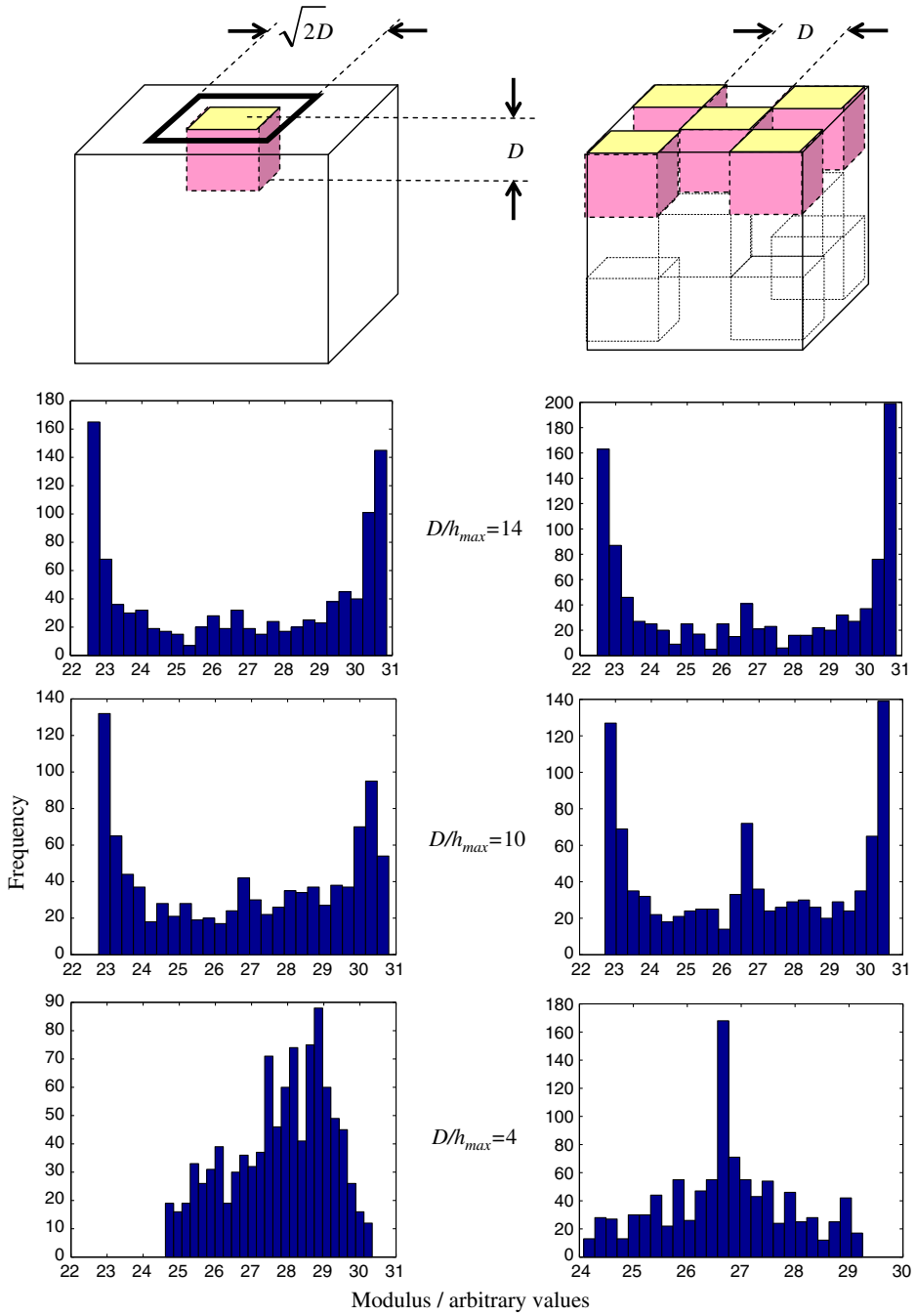

Fig. 4. Comparison of frequency plots for two different virtual microstructures: (left) matrix-inclusion morphology; (right) 3-D checkerboard. The figure illustrates that the appearance of a spurious peak is related to the choice of microstructure, and is not a general feature of the statistical nanoindentation technique, as postulated by Trtik et al. (2009).

(Fig. 2a), such that the computed contact depth-to-indentation depth ratio (h_c/h_{max})is close to the experimentally measured in cement paste nanoindentation, $h_c/h_{max} = 0.88$.

Finally, it should be noted that indentation tests are usually load-controlled and as a consequence indentation depths vary: we therefore experience lower indentation depths for indentations on stiff/hard phases, i.e. $h_{max} < 100$ nm in clinker phases, meaning that clinker phases larger than 1 μm can be identified with accuracy. Similarly, indentation depths in C–S–H phases are on the order of $h_{max} = 200 - 300$ nm, confirming that nanoindentation provides a means to determine the nanomechanical properties of LD C–S–H and HD C–S–H provided a characteristic size of hydration products greater than 2–3 μm. The question that needs then to be addressed is whether such homogeneous regions exist in hardened cement paste materials?

3. How homogeneous is cement paste microstructure?

Trtik et al.'s assertion, that no homogeneous domains of hydration products of micrometer size exist in hardened cement pastes, is based primarily on electron micrographs, which hinge on several core problems when interpreting micrographs that by nature can see only local structure at one scale. This issue deserves some

discussion, but first it should be noted that the proposed model of LD and HD C–S–H packing arrangements [29,30] was motivated to explain the surface area and density as measured using methods that probe different scales. The existence of at least two packing densities rationalizes a wide range of measured surface areas, with particular attention paid to those measured by nitrogen, which yields values that are particularly sensitive to the method used to dry a sample. The final model, now referred to as colloid model, also rationalizes measured densities as a function of water content. C–S–H is modeled as particles that pack together into two reasonably well defined packing arrangements, one with a packing density equal to closest packed spheres (26% pore) and the other with packing density of random jammed packed spheres (34% pore). These pores are the gel-pores. The particles are tiny, with a characteristic dimension of 5 nm, but the porosity is for the gel with dimensions that extend to the edge of the capillary pores, when, if saturated, has a composition of about 1.7 C–S–4H. The experimental and theoretical interpretation of nanoindentation experiments independently support the two packing densities with nearly the exact same predicted specific pore volumes [2,12,3]. This is very powerful all by itself. Trtik et al. raise the possibility that this agreement between models and experiments, which collectively agrees with a large amount of apparently disparate information is actually a coincidence. Their argument is based on a narrow interpretation of electron micrographs, but this does stimulate the legitimate question of the size of homogeneous regions. We very briefly review some observations that may help interpret electron micrographs, which amongst other things, require extensive preparation including drying that removes gel water and alters structure before observation.

Some of our understanding of the packing arrangement comes from neutron scattering experiments. Because the HD structure is very tightly packed with only very small pores between the particles it does not scatter neutrons, which only probe the LD structure. The LD structure is complex, possibly fractal at certain scales with a corresponding complex pores structure at various scales. It also both reversibly and irreversibly shrinks on drying with the most notable change an increase in packing density and a corresponding large reduction in the pores about 10 nm in diameter [12]. This shrinkage has been observed directly and clearly must be taken into account when interpreting electron micrographs that must be dried before polishing and placing into the microscope.

The electron micrographs of Richardson [28], referred to by Trtik et al., show little evidence for a relatively high volume of gel pores within the C–S–H boundaries, required by the colloid model, leading to the possibility that they are mostly removed during specimen preparation. If the gel pores are removed the larger capillary pores become larger. This is a problem with essentially all electron microscopic analysis.

The large shrinkage during drying complicates the problem of establishing the size of homogeneous regions using microscopic techniques. Pores that are evenly distributed move into the larger capillary pore region during drying. Furthermore the only pores that can be resolved individually by SEM are the larger capillary pores, the structure of which must be interpreted keeping in mind that drying removes pores from the gel and enlarges or even creates larger pores that may not even be present before drying. In spite of these limitations, images of polished surfaces using backscattered electrons have provided valuable insight.

Fig. 5a is a backscatter electron micrograph of a carefully prepared C3S paste. Micrographs like this are consistent with large regions (10's of microns or more) identified as phenograins and groundmass observed in portland cement paste. These very large regions speak to the reason that the colloid model introduced the terms LD and HD in order to separate from the idea that the densities are exclusively determined by the surface of the clinker particles when hydration begins. The concept of inner and outer product may be deceiving. Thus, a region of either HD or LD can be many 10's of microns across.

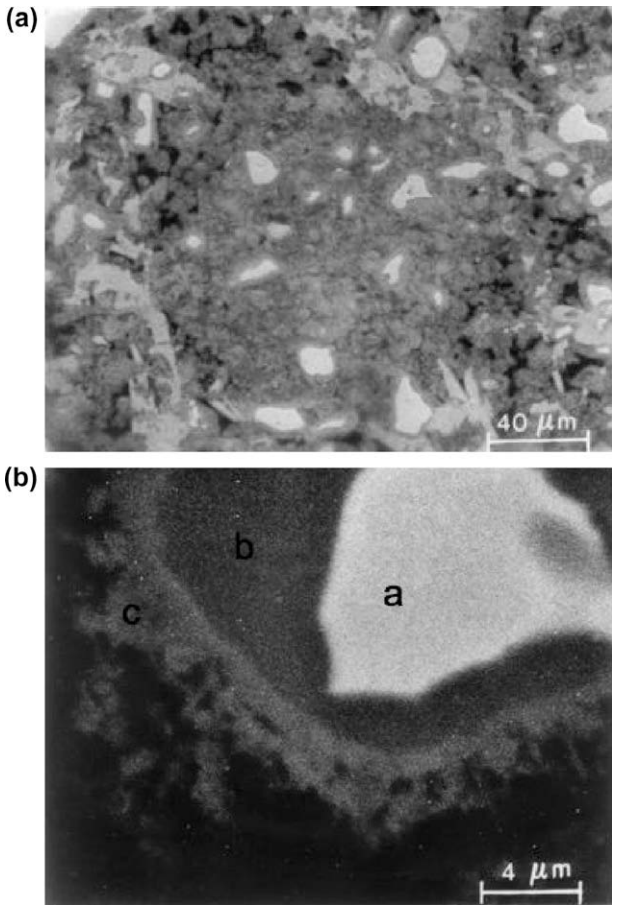

Fig. 5. Backscattered scanning electron micrographs of C3S paste of water/C3S= 0.5, hydrated for 28 days. Preparation included solvent exchange drying and filling the pores with low viscosity epoxy. Assignment of phases is white = C3S, light gray = CH, dark gray = C–S–H, and black = pore. The two micrographs show: (a) An overview of the microstructure with a large relatively dense region of C–S–H that engulfs many grains of C3S, with more porous regions in the surrounding area. This micrograph is chosen to emphasize the "phenograin" and "groundmass" parts of the microstructure, the sizes of which are not determined by the boundaries of the original C3S grains, and they extend many 10's of microns. The distribution of these regions is not represented by this micrograph, or any one micrograph and more of the porous structure is evident in other areas. (b) A relatively few grains exhibit a true "inner product" that still seems to preserve the general shape of the original grain. The reason for relative darkness of this region is unclear. These regions are rare at higher *w*/*c*.

A higher magnification micrograph, Fig. 5b, taken in a more open region and near an unreacted particle shows that the concept that at least some of the microstructure can be described by HD C–S–H surrounded by a rim of LD material sometimes holds. However, interestingly, if the LD is the more open regions in Fig. 5a and HD is the more dense region in the center of the micrograph, then this center region, which is not very abundant in this sample and is often of small cross section, may be a Ultra-High Density phase (UHD) more common in very low w/c samples [16]. These micrographs, along with many in the literature illustrate the complexity of the microstructure, and how different views are developed from observation at different scales. Certainly relying on TEM micrographs to define the size of a homogeneous region in a material with this complexity is risky, and there is abundant evidence that regions with distinct well defined density both help explain a large perplexing body of surface and density observation

and also, that they are large enough to be detected by nanoindentation techniques.

These observations are even more relevant to cements of very low water/cement ratio, where the UHD packing is more common and preparation of representative micrographs is easier. Homogeneous regions larger than a few microns are without question common [24]. Even in C3S pastes regions up to 20 μm in edge size are homogenous in composition. All of these arguments draw into question the fundamental premise of Trtik et al. that the different packing densities and associated moduli and hardnesses are actually artifacts with surprising agreement to models based on entirely independent data sets.

As far as nanoindentation is concerned, indentations operated to a depth of $h_{max} = 200$ nm, that activate material situated on a surface radius of $4 \times h_{max} = 800$ nm (see Fig. 2a), clearly probe the microstructure of a homogeneous material in the sense of Buckle's phase separability condition.

To further advance our argument, it may be useful to have a closer look at the chemical composition of the material domain probed by nanoindentation. This is achieved here with the chemical composition determined by Wavelength Dispersive Spectroscopy (WDS), which probes chemically a microvolume comparable in size, intensity and gradation to the interaction volume solicited mechanically by nanoindentation [25] (Fig. 6a). With a focus on

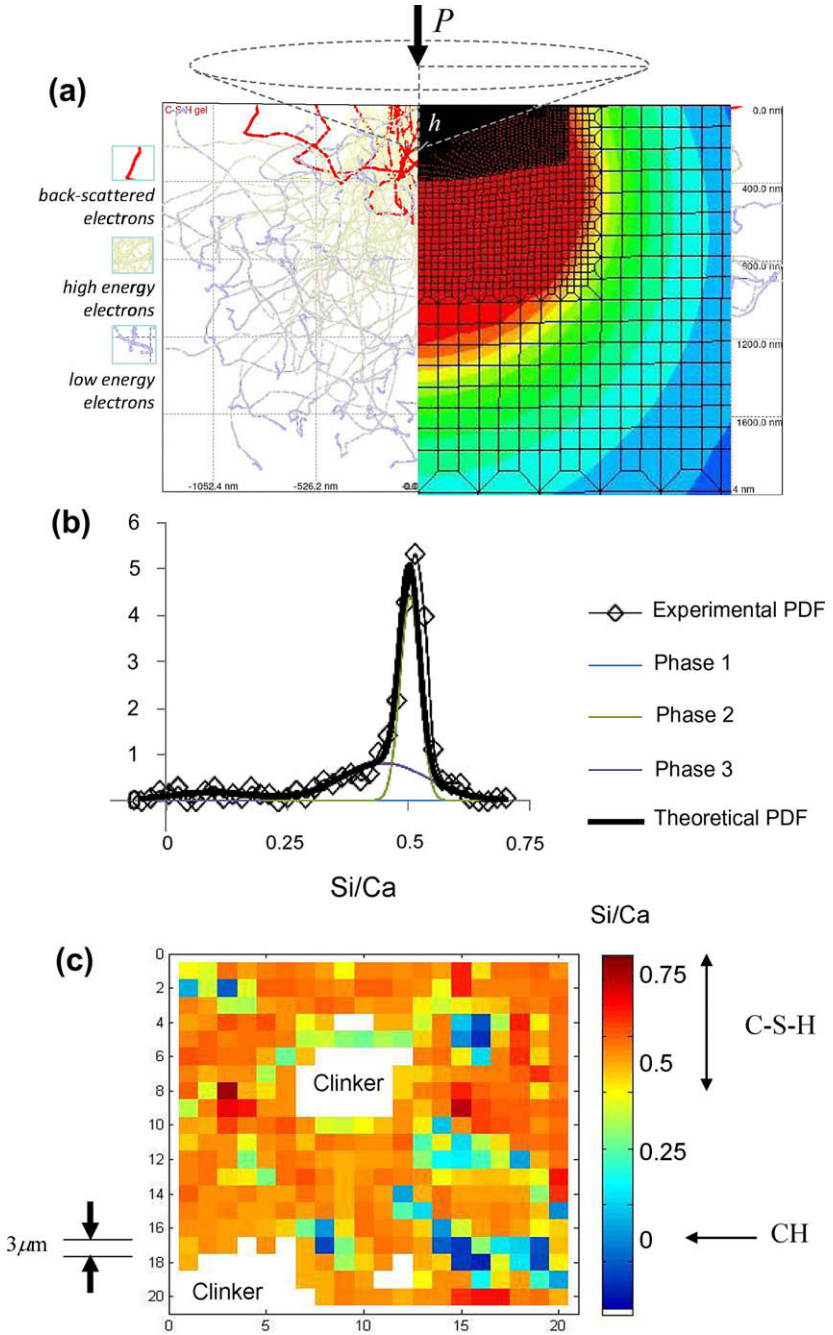

Fig. 6. (a) Interaction volumes probed respectively chemically by Wavelength Dispersive Spectroscopy (WDS) (left) and mechanically by nanoindentation (right): the left-half of the figure displays results of Monte Carlo simulation of electron beam penetration of C–S–H gel. The right-half represents finite element results of Von-Mises stresses below the indenter; (b) frequency plot and deconvolution of chemical composition (Si/Ca ratio) and (c) its mapping in a $w/c = 0.3$ hardened cement paste. Results from Wavelength Dispersive Spectroscopy on a grid with 3 μm spacing.

chemical composition distribution, we carried out a spot-WDS on the $w/c = 0.3$ hardened cement paste on a regular 20×20 grid of 3 μm spacing (same as Trtik et al. in their Fig. 9), which is large enough to minimize the overlap of adjacent microvolumes, and small enough to provide a snapshot of the chemical (elemental concentration) gradation on a real cement paste material. We then analyzed the results statistically, using a similar algorithm as for (M,H) via the Expectation–Maximization (EM) algorithm [26]; but now applied to the chemical experimental data set (Ca, Si, ...). This statistical compositional analysis is shown in Fig. 6b and c in form of a (molar) Si/Ca frequency plot of the hydration phases, and a spatial mapping of this chemical composition on a 3 μm grid. Both reveal that the hydration phases in real hardened cement pastes constitute compositionally homogeneous regions that are typically larger than a few microns, much in the same way as in nanoindentation (Fig. 1). This includes residual clinker phases and Calcium–Silicate–Hydrates (C–S–H), the dominant phase in these materials (there also exists a C–S–H/CH composite phase [27,25] recognized by a Si/Ca ratio situated between Si/Ca = 0 representing CH, and $0.4 < Si/Ca < 0.8$ representing the composition variation of 'pure' C–S–H in 'real' cement paste [28]).

Given this homogeneous chemical compositional distribution — at the characteristic length scale of nanoindentation as monitored through the indentation depth (see Fig. 6a)— we thus confirm our earlier suggestion [29,30] that C–S–H in real cementitious materials exists in (at least) two compositionally similar but structurally distinct forms that merely differ in the packing density of nanometer sized elementary particles [2]. The molecular structure and properties of C–S–H are now well known from model-based atomistic simulations [31], validated experimentally by statistical nanoindentation techniques and used successfully in the prediction of macroscopic stiffness and strength properties of cement-based materials [32,11,33–35]. Unfortunately, the authors' unvalidated micromechanical modeling of cement paste based on a FIB-nt dataset fails to implement these links between molecular properties, microstructure and mechanical properties, packing density distribution, mechanical phase allocation and interaction, scale separability, and finally a realistic strain gradation for stiffness homogenization.

Thus the assertions made in Trtik et al.'s article regarding statistical indentation analysis are groundless.

Acknowledgement

Support of MB through MIT's Undergraduate Research Opportunity Program in gratefully acknowledged.

References

[1] Constantinides G, Chandran KSR, Ulm F-J, Van Vliet KJ. Grid indentation analysis of composite microstructure and mechanics: principles and validation. Mater Sci Eng A–Struct Mater Prop Microstruct Process 2006;430(1–2):189–202.
[2] Constantinides G, Ulm F-J. The nanogranular nature of C–S–H. J Mech Phys Solids 2007;55(1):64–90.
[3] Ulm F-J, Vandamme M, Bobko C, Ortega JA, Tai K, Ortiz C. Statistical indentation techniques for hydrated nanocomposites: concrete, bone, and shale. J Am Ceram Soc 2007;90(9):2677–92.
[4] Randall NX, Vandamme M, Ulm F-J. Nanoindentation analysis as a two-dimensional tool for mapping the mechanical properties of complex surfaces. J Mater Res 2009;24(3):679–90.
[5] Buckle H. In: Westbrook JW, Conrad H, editors. The science of hardness testing and its applications. American Society for Metals, Metal Park OH; 1973. p. 453–91.
[6] Hertz H. Miscellaneous papers. London: Macmillan; 1896.
[7] Love AEH. The stress produced in a semi-infinite solid by pressure on part of the boundary. Philos Trans Roy Soc London Series A, Math Phys Sci 1929;228:377–420.
[8] Love AEH. Boussinesq's problem for a rigid cone. Quart J Math 1939;10: 161–75.
[9] Galin LA. Contact problems in the theory of elasticity. Moscow: Gostekhizdat; 1953.
[10] Sneddon IN. The relation between load and penetration in the axisymmetric Boussinesq problem for a punch of arbitrary profile. Int J Eng Sci 1965;3(1): 47–57.
[11] Constantinides G, Ulm F-J. The effect of two types of C–S–H on the elasticity of cement-based materials: results from nanoindentation and micromechanical modeling. Cement Concrete Res 2004;34(1):67–80.
[12] Jennings HM, Thomas JJ, Gevrenov JS, Constantinides G, Ulm F-J. A multi-technique investigation of the nanoporosity of cement paste. Cement Concrete Res 2007;37(3):329–36.
[13] Miller M, Bobko C, Vandamme M, Ulm F-J. Surface roughness criteria for cement paste nanoindentation. Cement Concrete Res 2008;38(4):467–76.
[14] Dormieux L, Kondo D, Ulm F-J. Microporomechanics. Chichester, UK: J Wiley & Sons; 2006.
[15] DeJong MJ, Ulm F-J. The nanogranular behavior of C–S–H at elevated temperatures (up to 700 degrees C). Cement Concrete Res 2007;37(1):1–12.
[16] Vandamme M, Ulm F-J. Nanogranular origin of concrete creep. Proc Nat Acad Sci USA 2009;106(26):10552–7.
[17] Tai K, Ulm F-J, Ortiz C. Nanogranular origins of the strength of bone. Nano letters 2006;6(11):2520–5.
[18] Ulm F-J, Abousleiman Y. The nanogranular nature of shale. Acta Geotech 2006;1(3):77–88.
[19] Bobko C, Ulm F-J. The nano-mechanical morphology of shale. Mech Mater 2008;40(4-5):318–37.
[20] Cheng YT, Cheng CM. Scaling, dimensional analysis, and indentation measurements. Mater Sci Eng R-Reports 2004;44(4–5):91–149.
[21] Ganneau FP, Constantinides G, Ulm F-J. Dual-indentation technique for the assessment of strength properties of cohesive-frictional materials. Int J Solids Struct 2006;43(6):1727–45.
[22] Cariou S, Ulm F-J, Dormieux L. Hardness-packing density scaling relations for cohesive-frictional porous materials. J Mech Phys Solids 2008;56(3):924–52.
[23] Durst K, Goken M, Vehoff M. Finite element study for nanoindentation measurements of two-phase materials. J Mater Res 2004;19(1):85–93.
[24] Diamond S, Bonen D. Microstructure of hardened cement paste – a new interpretation. J Am Ceram Soc 1993;76(12):2993–9.
[25] Chen JJ, Sorelli L, Vandamme M, Ulm F-J, Chanvillard G. A coupled grid-indentation/SEM-EDX study on low water/cement ratio Portland cement paste: evidence for C–S–H/CH nanocomposites, J Am Ceram Soc; submitted for publication.
[26] McLachlan GJ, Peel D, Basford KE, Adams P. The EMMIX software for the fitting of mixtures of normal and *t*-components. J Stat Softw 1999; 4(2). <www.maths.uq.edu.au/gjm/emmix/emmix.html>.
[27] Allen AJ, Thomas JJ, Jennings HM. Composition and density of nanoscale calcium–silicate–hydrate in cement. Nat Mater 2007;6:311–6.
[28] Richardson IG. The nature of C–S–H in hardened cements. Cement Concrete Res 1999;29:1131–47.
[29] Jennings HM. A model for the microstructure of calcium silicate hydrate in cement paste. Cement Concrete Research 2000;30:101.
[30] Jennings HM. Refinements to colloid model of C–S–H in cement: CM-II. Cement Concrete Res 2008;38(3):275–89.
[31] Pellenq RJ-M, Kushima A, Shahsavari R, Van Vliet KJ, Buehler MJ, Yip S, et al. A realistic molecular model of cement hydrates. In: Proc Nat Acad Sci USA 2009;106: Early Edition Sep 7 2009. Available from: www.pnas.orgcgidoi10.1073pnas.0902180106.
[32] Bernard O, Ulm F-J, Lemarchand E. A multiscale micromechanics-hydration model for the early-age elastic properties of cement-based materials. Cement Concrete Res 2003;33(9):1293–309.
[33] Ulm F-J, Constantinides G, Heukamp FH. Is concrete a poromechanics material? – a multiscale investigation of poroelastic properties. Mater Struct 2004;37(265):43–58.
[34] Ganneau FP, Ulm F-J, Gondzio J, Garboczi EJ. An algorithm for computing the compressive strength of heterogeneous cohesive-frictional materials – application to cement paste. Comput Geotech 2007;34(4):254–66.
[35] Sorelli L, Constantinides G, Ulm F-J, Toutlemonde F. The nano-mechanical signature of Ultra High Performance Concrete by statistical nanoindentation techniques. Cement Concrete Res 2008;38(12):1447–56.